Experimental Thermal and Fluid Science 166 (2025) 111482

Contents lists available at ScienceDirect

Experimental Thermal and Fluid Science

journal homepage: www.elsevier.com/locate/etfs

Experimental investigation of unsteady fan-intake interactions using time-resolved stereoscopic particle image velocimetry

Matteo Migliorini *, Pavlos K. Zachos, David G. MacManus, Alexandros Giannouloudis

Centre for Propulsion and Thermal Power Engineering, Faculty of Engineering and Applied Sciences, Cranfield University, UK

A B S T R A C T

Understanding engine response to unsteady intake flow distortion is a crucial requirement to de-risk the development of novel aircraft configurations. This is more critical for configurations with highly embedded engines. Recent advances in non-intrusive, laser-based flow diagnostics demonstrated the ability to measure unsteady flows in convoluted intakes with high resolution in time and space. This work presents novel non-intrusive, unsteady flow measurements ahead of a fan rotor coupled to a convoluted diffusive intake. The fan rotor caused a local increase of the maximum levels of swirl intensity at the blade tip region, as well as flow redistribution at the interface plane between the fan and the inlet duct compared to the baseline configuration with no fan in place. This contributed to the reduction of the overall swirl angle unsteadiness across the main flow distortion frequencies. This research presents a notable advance in unsteady fan-intake interaction characterisation. The work shows that high-resolution optical measurements offer notably better understanding of these complex aerodynamic interactions and have the potential to be part of larger scale, industrial testing programmes for future product development and certification.

1. Introduction

In the last decade there has been a notable focus on the development of new aircraft designs such as Blended-Wing-Body (BWB) and Boundary Layer Ingesting (BLI) engine configuration which could help address the need for fuel burn reduction [1–3]. In these configurations, convoluted intakes are expected to be used for the integration of the propulsion system with the fuselage. Although these configurations have potential advantages for overall fuel burn reduction, there is an acknowledged vital concern regarding unsteady flow distortion [4], which can adversely affect the propulsion system performance [5] and its aerodynamic and mechanical stability [6–9]. A key aspect to enable the development of these novel aircraft architectures is the capability to measure and characterise the unsteady flow distortions and to evaluate the impact on the fan system. This is also relevant in the context of the design of closely coupled diffusers [10–12]. Intrusive methods used in industry-standard measurement systems use probes which do not provide adequate spatial resolution of the flow distortion.

Several previous studies have characterised the unsteady flows in convoluted diffusers using non-intrusive measurement methods such as stereoscopic particle image velocimetry (SPIV). These methods provide high resolution and synchronous velocity measurements across an aerodynamic interface plane (AIP) and were successfully used to characterize the unsteady flow distortion at the exit of complex diffusers [13–19]. This has also enabled the development of novel methods to evaluate the magnitude and extent of the unsteady distortion events [20]. Unsteady distortion measurements with SPIV were recently demonstrated for a podded, aspirated civil inlet operating at cross-wind conditions at an industrial wind-tunnel environment [21].

In most of these previous studies the intakes were un-coupled from a fan. This is mainly due to the difficulties arising from the application of high-resolution optical measurement techniques fan intake configurations. These difficulties are mainly linked to the need of enabling high-quality optical access while through non-parallel intake walls to allow for closely-coupled fan-intake configuration, the vibrations induced by the fan, and the spurious data generated by unsteady reflections caused by rotating blades in the background. Only limited published studies reported successful measurements with coupled intake-fan systems. Guimarães et al. [22] measured flow distortion from a distortion gauze installed at the inlet of a research turbofan engine by combining separate measurements of 30 degrees angular sectors across the AIP plane. More recently, Piovesan et al. [23] demonstrated coupled-fan intake flow distortion measurements of a podded engine at crosswind conditions, with synchronous multi-camera measurements to capture the full AIP plane at once. However, there is strong evidence that the presence of a fan influences the characteristics of the unsteady flow within the inlet system. For example, experimental investigations on civil, high-bypass intakes demonstrated that the presence of the fan attenuated instabilities arising from the intake lip separations and allowed the operation of the intake with higher angles of attack [24–28]. Conversely, recent computational studies revealed that the additional unsteadiness

* Corresponding author.
E-mail address: matteo.migliorini@cranfield.ac.uk (M. Migliorini).

https://doi.org/10.1016/j.expthermflusci.2025.111482
Received 20 January 2025; Received in revised form 6 March 2025; Accepted 21 March 2025
Available online 24 March 2025

Nomenclature

AIP	Aerodynamic Interface Plane
BLI	Boundary Layer Ingesting
BWB	Blended-Wing-Body
CCITF	Cranfield Complex Intake Test Facility
D	Diameter, m
EDF	Electric Ducted Fan
ESC	Electronic Speed Controller
f	Frequency, Hz
M	Mach number
P	Probability
PDF	Probability Density Function
PIV	Particle Image Velocimetry
r	Radial coordinate, m
R	Radius, m
SAE	Society of Automotive Engineers
SD	Swirl Directivity
SI	Swirl Intensity, deg
SP	Swirl Pairs
SPIV	Stereo Particle Image Velocimetry
St	Strouhal number
TR	Time-resolved
var	Variance
V	Velocity component, m/s
X	Horizontal coordinate
Y	Vertical coordinate
Z	Streamwise coordinate
α	Swirl angle, deg
ω	Rotational speed, rpm
$\langle\,\rangle$	Time-averaged
–	Area-averaged

generated by the rotating fan can produce adverse effects on the intake separation characteristics [29]. Hence time-resolved, high-resolution measurement capability to characterise coupled fan-intake systems is important.

This work presents unsteady flow distortion measurements ahead of a fan rotor closely integrated downstream of an S-shaped diffuser. Time resolved SPIV (TR-SPIV) was used to measure the dynamic swirl distortions at a cross-flow plane located upstream of the rotor inlet plane. The measurements of the coupled configuration are compared against a baseline case where the intake was aspirated without the fan in place.

2. Experimental setup and data processing methods

Coupled fan-intake experiments were conducted within the Cranfield Complex Intake Test Facility (CCITF, Fig. 1). The rig comprises a bell mouth inlet, a flow straightening section, a nozzle, a cylindrical inlet section, and an S-duct diffuser with a diameter of 160 mm at the Aerodynamic Interface Plane (AIP). The S-duct is a scaled version of a convoluted diffuser previously studied by Garnier et al. [30] with a diffusing area ratio of 1.52 and offset to length ratio of 0.49. A detailed description is reported by Migliorini et al. [31]. This S-duct diffuser was coupled with an Electric Ducted Fan (EDF) Vasyfan model VF-160 powered by a high-speed brushless DC motor. The fan had 10 rotor blades with a diameter of 158 mm at the inlet and maximum operating speed of 25,000 rpm. At this speed, the blade tip Mach number approximately 0.6. It is acknowledged that this is not fully representative of typical transonic fan, however this can be used to establish the experimental technique to enable coupled-intake fan assessments. The Mach number range at the centreline of the inlet of convoluted diffuser was between M_{ref} = 0.07 – 0.36 measured 0.66 D_{AIP} upstream of the S-duct inlet (inlet reference plane in Fig. 1). The fan was powered by a 24 kW AC-DC rectifier which provides up to 200A at 120VDC to the Electronic Speed Controller (ESC) (Fig. 1). The experiments were conducted at inlet Mach numbers of 0.18, 0.27 and 0.36 with fan speeds of 12,500, 18,500 and 24,000 rpm respectively.

For the comparative analysis, the AIP flow field was also assessed without the EDF in place. In this configuration the diffuser was aspirated through a conical diffuser by a suction fan installed approximately 16.3D_{AIP} downstream of the measurement plane to eliminate any interference. The speed of the suction fan was modulated to match the inlet Mach number M_{ref} = 0.18, 0.27, and 0.36 at the inlet reference plane (Fig. 1) to enable comparisons with the configuration with the EDF.

Time-Resolved, Stereo-Particle Image Velocimetry (TR-SPIV) was used to measure the unsteady flow distortion at the AIP. A pair of CMOS cameras with a sensor resolution of 1280 × 800 px was used for imaging. The left camera was equipped with a Nikkor f/2.8 60 mm lens, while the right camera was equipped with a Nikkor f/2.8 60 mm lens. Both cameras were equipped with Scheimpflug mounts for focus correction across the AIP plane. The flow was seeded with DEHS seeding particles

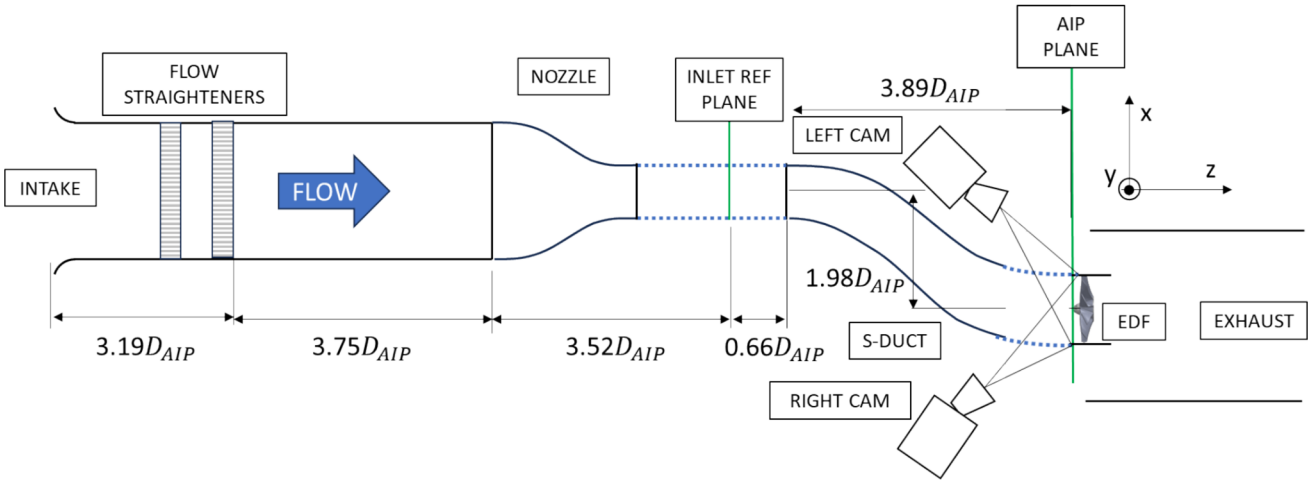

Fig. 1. Plan-view schematic of the Cranfield Complex Intake Test Facility (CCITF) with the Electric Ducted Fan (EDF) closely coupled to a convoluted diffusive intake duct (top view). Dotted lines indicate the optical walls for non-intrusive measurements.

with a mean diameter of 1 μm. The measurements were conducted at the exit plane of the S-duct diffuser (AIP plane, Fig. 1). A light sheet generated by a pulsed Nd:YAG laser was delivered at this location. A dataset comprising 20,000 velocity flow-fields was captured with a temporal frequency of 8 kHz, which provided between 2 and 4 velocity fields for each blade passing. The time-delay between pulses was adjusted in a range between approximately 3 and 6 μs as a function of M_{ref} in accordance with PIV cross-correlation principles [32]. The AIP was approximately 0.12 D_{AIP} upstream the EDF fan face. The final processing of the SPIV measurements yielded a spatial resolution at 2.3 mm × 2.3 mm on a 160 mm diameter AIP, which resulted in approximately 3,000 3D velocity vectors across the plane. The data was processed with the commercial software LaVision Davis ver. 10.2.1. After processing, only regions within 90 % of the AIP radius were considered to avoid spurious velocity vectors induced by laser light reflections. The uncertainty of the velocity components is 3.3 % of the area-averaged, time-averaged streamwise velocity at the AIP based on the method of Raffel et. al. [32].

The optical access was evaluated by assessing the line of sight of two PIV cameras of the exit portion of S-duct intake with the intent to optimize the axial length of the transparent walls of the S-duct intake upstream the fan face. This produced an improvement of the technique as it reduced the optical distortions when imaging through non-parallel walls of the S-duct intake. A further improvement of the technique was the use of high-absorption, matt-back paint with to reduce the unsteady reflections caused by rotating blades. To keep the stereo half angle to a reasonable low aperture, the camera on the port side was lowered along the y axis relative to the S-duct centreline to compensate for the reduced spatial clearance available near the first S-duct bend (left camera, Fig. 1). The starboard camera was aligned with the rig centreline along the y-axis. This setup slightly compromised the line of sight around the nose cone. The use of additional cameras would improve the optical line of sight of regions near the spinner [23], however these were not available during this experimental campaign. The fan spinner imposed additional challenges to the PIV measurements at the fan face. High-intensity and unsteady laser light reflections were observed in the region around the spinner with a detrimental effect to the local signal to noise ratio. This generated areas at the AIP where no velocity data was obtained. This data loss is generally unavoidable in a two-camera setup, but can be substantially reduced with multi-view camera systems [21,31]. Due to this optical setup (Fig. 1), these areas were not symmetric with respect to the spinner. The extent of these regimes was evaluated with the distribution of the time-averaged streamwise velocity uncertainty computed with Wieneke's method [33]. The velocity uncertainty has been obtained PIV cross-correlation of the whole AIP plane. The resulting area with high uncertainty has been approximated with an ellipse with centre in $X = 0.1\ r/R_{AIP}$ and $Y = 0.1\ r/R_{AIP}$ and with main axis $a_x = 0.35\ r/R_{AIP}$ and $b_y = 0.25\ r/R_{AIP}$. The velocity vectors within this ellipse have been excluded from the analysis in a post-processing step. The additional areas with high velocity uncertainty in the lower right corner are attributed to a combination of laser light reflections due to the AIP curvature and optical distortion caused by the bends in the S-duct walls, which could not be avoided. The laser light also created additional reflections in the left side of the domain boundary. This imposes limitations of the study on the higher spanwise region of the blades beyond r/R = 0.90.

3. Results and discussion

Unsteady flow measurements were conducted for two experimental configurations: aspirated and with a closely-coupled EDF rotor at the exit of the S-duct diffuser. The analysis of the flow distortion characteristics showed that the effects of the fan were broadly the same across the range of fan operating speed. The EDF is a subsonic, stator-less fan and does not generate shock waves that typically influence the flow field upstream of the rotor's leading edge. Thus, the analysis focused mainly on the operating point at $M_{ref} = 0.36$. The velocity distributions are normalized against the area-averaged, time-averaged streamwise velocity component (V_Z) of the aspirated S-duct configuration to enable comparisons.

The distribution of the streamwise velocity component V_Z shows an area of high momentum on the right-hand side of the domain, which corresponds to the outward wall of the first S-duct bend (Fig. 2a). The low momentum region on the left-hand side of the domain (Fig. 2a) is linked with the typical S-duct secondary flows. This is influenced by the presence of the rotor blades and the spinner, which promote the streamwise flow uniformity by mass re-distribution across the plane. Indeed, the streamwise velocity on the left side of the domain increases (Fig. 2e) compared to the aspirated S-duct configuration (Fig. 2a). An increase of the radial velocity V_r towards positive values is also observed across the full AIP plane for the coupled configuration (Fig. 2g). It is envisaged this is due to the combined presence of a spinner and EDF motor casing, which deflect the flow radially towards the duct outer boundaries. This is consistent with previous investigations on the effect of a centrebody on the S-duct intake flow distortion [34]. The swirl angle distribution is only mildly influenced by the presence of the fan. The swirl angle is biased towards negative values primarily in the left side of the domain, where there is low momentum flow (Fig. 2f), compared with the baseline case with no fan (Fig. 2b). This effect is consistent with the definition of the swirl angle, which is positive in the counter-clockwise direction, whist the fan is spinning in the counter-clockwise direction.

A typical flow feature found in the time −averaged velocity field of single offset S-duct diffusers is a twin-paired counter-rotating vortex structure (left part of the AIP − Fig. 2b). This twin-swirl pattern was not found to be significantly influenced by the presence of the fan rotor. Nevertheless, the fan rotor causes a flow bias towards negative angles (swirl angle is positive in the counter-clockwise direction), opposite to the fan rotation (Fig. 2f). However, the maximum values of the time-averaged swirl angle distribution (Fig. 2c, Fig. 2g), and the underpinning swirl angle unsteadiness (Fig. 2d) is mostly unaffected by the presence of the rotor (Fig. 2d, Fig. 2h).

In terms of swirl distortion, the industry-standard swirl distortion metrics were computed, to characterize the swirl intensity (SI), number of swirl pairs (SP) and swirl directivity (SD) for the aspirated and the configuration with the fan rotor in place [35]. These descriptors are calculated on data interpolated on 5 equal-area rings corresponding to typical 5x8 probe arrangement according to the Aerospace Recommended Practice ARP1420 [36]. These descriptors are analysed in pairs with joint-probability density function maps to assess the unsteadiness of swirling structures in time [17,19]. These are computed with the following formula:

$$P(SI_A \le SI \le SI_B, SP_A \le SP \le SP_B) = \int_{SP_A}^{SP_B}\int_{SD_A}^{SD_B} PDFdSDdSP \quad (1)$$

where $P()$ is the probability function of a swirl distortion topology with Swirl Intensity (SI) in the range between SI_A and SI_B, and Swirl Pairs (SP) in the range between SI_A and SI_B, with A and B representing the discretization of the SI-SP grid with a resolution of 0.03 for both descriptors.

The unsteady swirl angle distributions enabled the combined assessment of the swirl angle magnitude (SI) and the associated topology (SP, SD). Particular attention should be given to instantaneous individuals with high swirl intensity. These potentially change the local blade loading and could result in local aerodynamic or aero-mechanical off-design operation at parts of the fan blade [37]. The current analysis focused on two radial positions at r/R = 0.84 (Fig. 3) and r/R = 0.71 (Fig. 4), which correspond to 4th and 3rd ring of the industry-standard 40-probe equal-area distortion rake prescribed in the ARP1420,

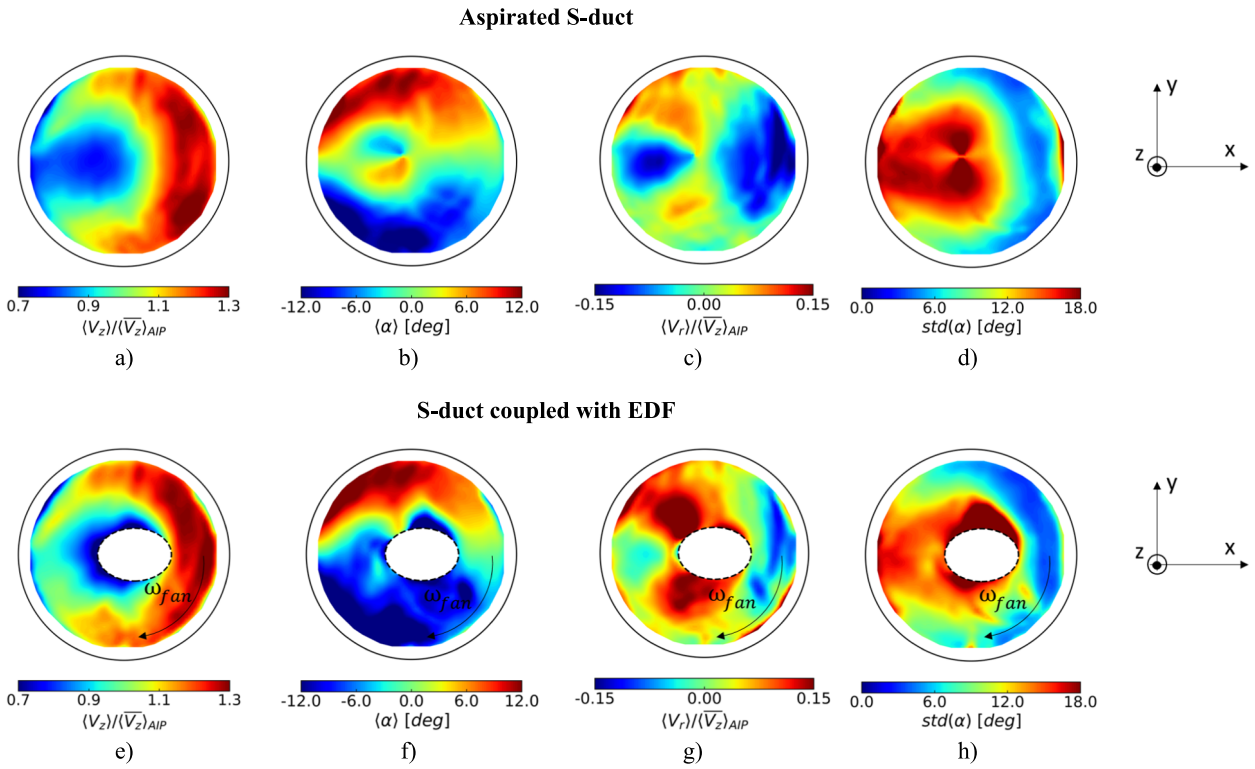

Fig. 2. Distribution of time-averaged a-e) streamwise velocity component V_Z, b-d) swirl angle α, c-g) radial velocity V_r, and d-h) swirl angle unsteadiness std(α) at the AIP for aspirated (top) and closely-coupled configurations (bottom) at $M_{ref} = 0.36$. Blank region contains spurious data. View looking upstream.

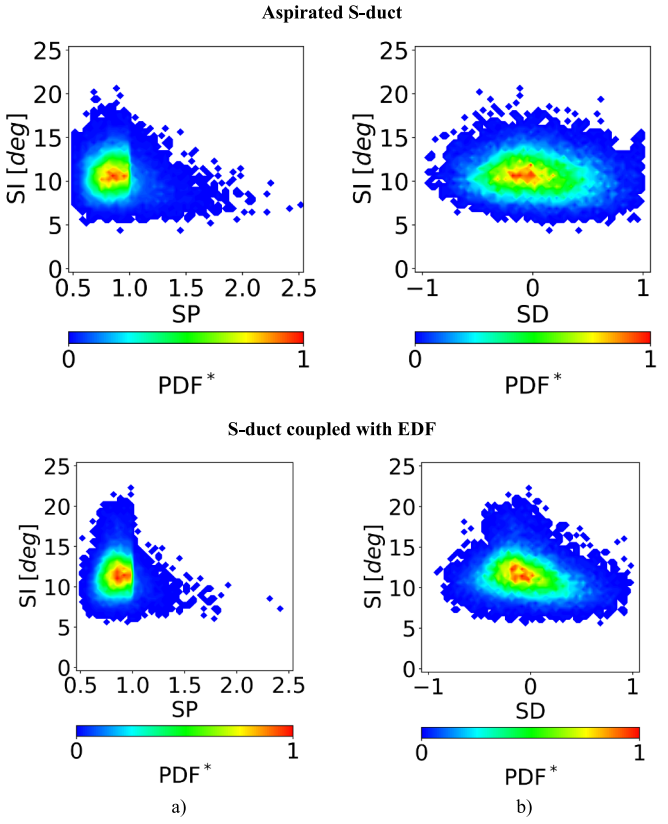

Fig. 3. a) j-PDF distribution of Swirl Intensity (SI) and Swirl Pairs (SP) and b) Swirl Intensity (SI) and Swirl Directivity (SD) measured at r/R = 0.84 for aspirated and closely-coupled configurations at $M_{ref} = 0.36$.

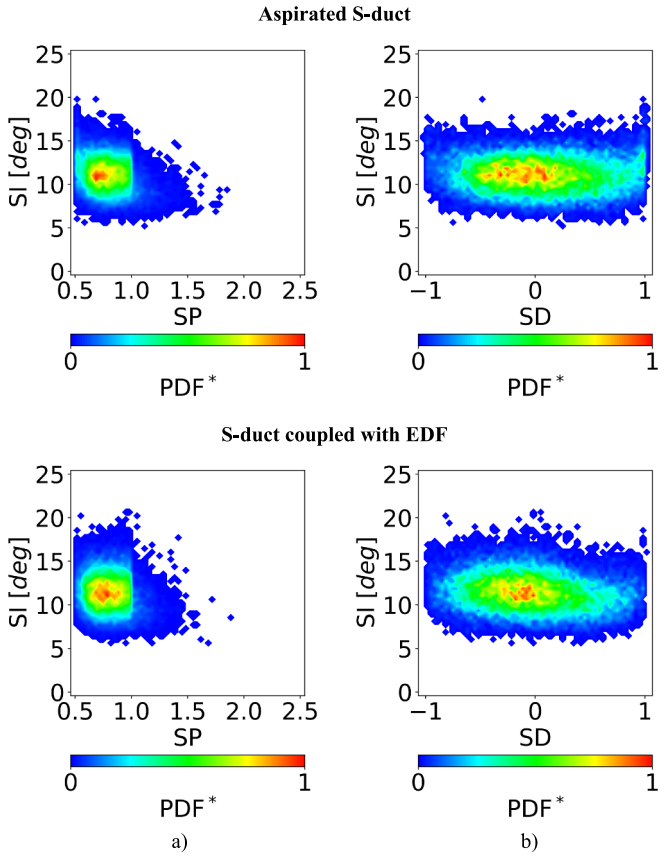

Fig. 4. a) j-PDF distribution of Swirl Intensity (SI) and Swirl Pairs (SP), and b) Swirl Intensity (SI) and Swirl Directivity (SD) measured at r/R = 0.71 for aspirated and closely-coupled configurations at $\boldsymbol{M_{ref}} = 0.36$.

respectively [36]. These are representative of the typical blade tip and peak blade loading region of typical transonic fans, which are of particular interest for aero-mechanical compatibility and the formation of stall cells [38]. These two radial locations fall in the annular portion beyond the elliptical region of excluded data around the spinner (Fig. 2). Radial locations closer to the spinner have been excluded from the analysis to avoid spurious vectors due to residual reflections from the spinner. The fan rotor caused an increase of the maximum SI by approximately 3.5° at the outer region (r/R = 0.84, Fig. 3) while it increased by 1.5° at r/R = 0.71, (Fig. 4) in relation to the aspirated configuration. This is a worsening operating condition for the fan rotor, as it is linked with higher incidence angles which could promote the development of stall cells [38,39].

The presence of the fan rotor also increased the relative frequency of twin-swirl distortion events (SD = 0) while, conversely, reduce the number of single bulk swirl patterns (SD = ±1). This is visible by comparing the peak swirl events in the SI-SD maps (Figs. 3b and 4b). In a previous study by Mehdi [40], it was found that bulk swirl events can have a higher impact on the reduction of the compressor surge margin compared to multiple pair swirl.

For the operating point at M_{ref} = 0.27, at r/R = 0.84 and at r/R = 0.71 the SI increased by approximately 3° in the presence of the EDF compared with the aspirated S-duct configuration (Fig. 5). At M_{ref} = 0.18, the maximum SI remained approximately constant at r/R = 0.84 between the aspirated and the EDF configuration, while it decreased slightly by 1.5° at r/R = 0.71. The levels of peak swirl distortion across the range of operating conditions are slightly increasing, mainly at the region near the blade tip, indicating that the fan rotor has a limited effect on the overall peak swirl distortion characteristics of the inlet diffuser.

The spectral signature of the swirl angle fluctuations was also studied. This method was previously used by Migliorini et al. [19] to identify the effect of non-uniform inlet conditions on the inherent S-duct flow distortion. This analysis uses an averaged periodogram method [41] in which the PIV dataset has been divided into 20 parts and a Hann window has been introduced to reduce frequency leakage. The frequency bands are defined on the Strouhal number $St = fD_{AIP}/\langle\overline{V_Z}\rangle$ where f is the frequency of the fluctuations, D_{AIP} the diameter of the AIP, and $\langle\overline{V_Z}\rangle$ the time-averaged, area-averaged streamwise velocity at the AIP. Each contribution is normalized by the overall area-averaged value of the swirl angle variance across each frequency band in the aspirated S-duct configuration, which allows comparisons on the relative magnitude of the spectra in the two configurations (Fig. 6). Based on the Nyquist criterion, frequencies up to about St = 8.0 can be determined for an acquisition frequency of 8 kHz. This is far greater than typical swirl angle fluctuations of this S-duct intake, which are typically in a range betweenSt = [0.2, 1.2] for uniform inlet flow conditions [19]. The strongest contribution is noted in a band betweenSt = [0.4, 0.6] (Fig. 6), which includes the swirl switching mode and corresponds to the alternation of positive and negative bulk swirl and twin-paired swirl patterns, as previously established by Gil-Prieto et al. [17]. With the presence of the fan rotor, the contribution of this switching mode atSt = [0.4, 0.6] still the dominant feature (Fig. 6). This was partially expected as the analysis of the swirl distortion through the descriptors highlighted a population of swirl patterns spanning between negative bulk (SD = −1), twin swirl (SD = 0), and positive bulk swirl (SD = 1) (Figs. 3b and 4b). The spectral analysis confirms that the swirl switching mode still occurs at the reference Strouhal number band. Overall, a slight decrease of the magnitude of the swirl fluctuations is observed across all the frequency bands for the close-coupled EDF S-duct configuration relative to the aspirated S-duct configuration (Fig. 6). The variance reduced especially in the left area of the AIP where the main vortical structures of the flow reside, and this is considered to be a stabilizing effect.

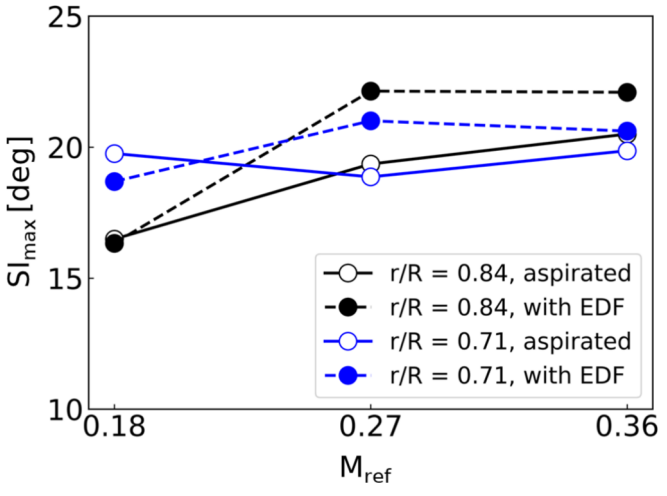

Fig. 5. Comparison of the time-averaged Swirl Intensity (SI) at ring locations r/R = 0.71 and 0.84 for aspirated and closely-coupled EDF configurations across a range of operating points.

4. Conclusions

This work demonstrates novel capability to perform non-intrusive, unsteady flow distortion measurements for coupled intake-fan configurations. The application of TR-SPIV to measure flow distortion ahead of a fan rotor coupled to a convoluted diffuser has never been shown to date. This is a major step forward for ability to characterise unsteady intake-fan interactions. Overall, for this specific configuration, the fan rotor effects on the flow distortion were relatively benign. S-duct inlet Mach number was only found to weakly influence the fan face distortion characteristics across the tested range. The experiments indicated a localized increase of peak swirl intensity at locations near the blade tip, and a radial flow re-distribution in the area associated with secondary flow structures. However, the unsteady effects of rotating blades on inlet flow characteristics are expected to be more prominent for typical transonic fans, and this is still an open research question in the community. The main contribution of this work is the demonstration of an experimental methodology to assess unsteady fan effects on inherent distortions of convoluted intakes. This level of detail in flow field velocity measurement would not have been possible with conventional, intrusive methods, whose inability to capture such detailed flow features yielded significant difficulties in past industrial programmes. The current work is a step forward in providing advanced experimental capability to characterise the complex flow fields and dynamic distortions at a fan-face that can support the design and integration of future propulsion systems.

Funding sources

The SINATRA project leading to this publication has received funding from the Clean Sky 2 Joint Undertaking (JU) under grant agreement No 886521. The JU receives support from the European Union's Horizon 2020 research and innovation programme and the Clean Sky 2 JU members other than the Union.

CRediT authorship contribution statement

Matteo Migliorini: Writing – review & editing, Writing – original draft, Visualization, Validation, Supervision, Software, Resources, Project administration, Methodology, Investigation, Formal analysis, Data curation, Conceptualization. **Pavlos K. Zachos:** Writing – review & editing, Supervision, Resources, Project administration, Funding acquisition. **David G. MacManus:** Writing – review & editing. **Alexandros Giannouloudis:** Investigation.

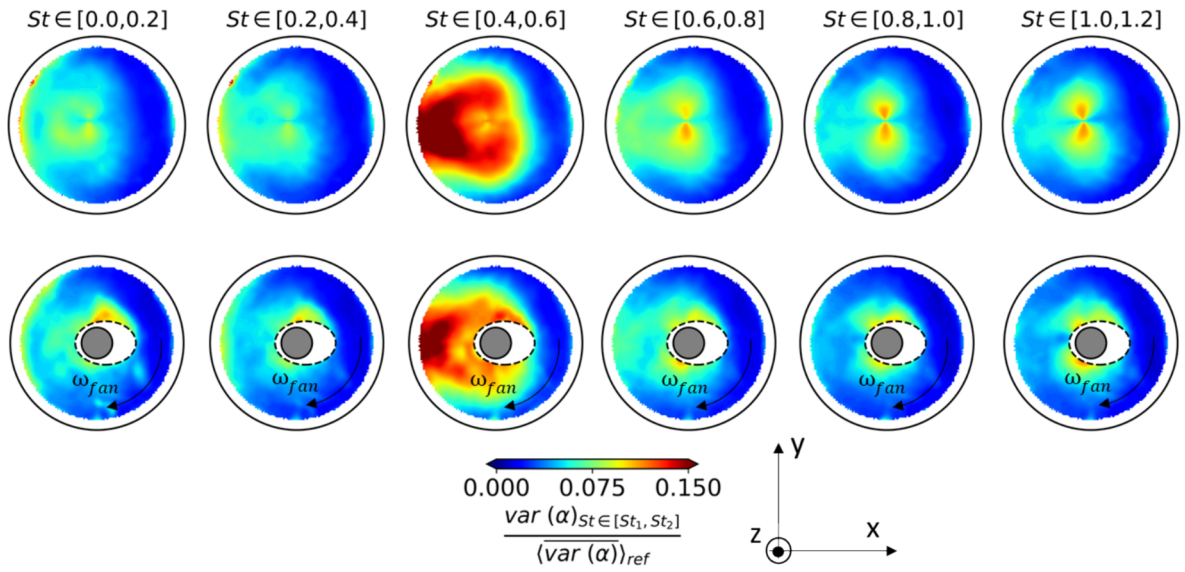

Fig. 6. Spectral signature of swirl angle (α) fluctuations arranged in bands of Strouhal number $\Delta St = 0.2$ for aspirated (top) and closely-coupled configurations (bottom) at $M_{ref} = 0.36$. Blank region contains spurious data. View looking upstream.

Declaration of competing interest

The authors declare that they have no known competing financial interests or personal relationships that could have appeared to influence the work reported in this paper.

Acknowledgements

The authors would like to thank Vasyfan for technical consultations on the EDF unit to enable the rig integration.

Data availability

Data supporting this study cannot be made available due to commercial confidentiality agreements.

References

[1] ACARE, Flightpath 2050, Europe's Vision for Aviation, Publications Office of the European Union, Luxembourg, 2012, doi: 10.2777/50266.
[2] A.H. Epstein, Aeropropulsion for commercial aviation in the twenty-first century and research directions needed, AIAA J. 52 (5) (2014) 901–911, https://doi.org/10.2514/1.J052713.
[3] P. Okonkwo, H. Smith, Review of evolving trends in blended wing body aircraft design, Prog. Aerosp. Sci. 82 (2016) 1–23, https://doi.org/10.1016/j.paerosci.2015.12.002.
[4] W.T. Cousins, History, Philosophy, Physics, and Future Directions of Aircraft Propulsion System/Inlet Integration, Vol. 2, 2004, pp. 305–320, doi: 10.1115/GT2004-54210.
[5] H.C. Melick Jr., Analysis of Inlet Flow Distortion and Turbulence Effects on Compressor Stability, Dallas, TX, US, 1973.
[6] H. Im, G. Zha, Investigation of flow instability mechanism causing compressor rotor-blade nonsynchronous vibration, AIAA J. 52 (9) (2014) 2019–2031, https://doi.org/10.2514/1.J052781.
[7] A. Kammerer, R.S. Abhari, Experimental study on impeller blade vibration during resonance—Part I: blade vibration due to inlet flow distortion, J. Eng. Gas Turbines Power 131 (2) (2009) 11, https://doi.org/10.1115/1.2968869.
[8] R. Chue, T.P. Hynes, E.M. Greitzer, C.S. Tan, J.P. Longley, Calculations of inlet distortion induced compressor flow field instability, Int. J. Heat Fluid Flow 10 (3) (1989) 211–223, https://doi.org/10.1016/0142-727X(89)90040-4.
[9] H. Mårtensson, M. Billson, Unsteady aerodynamic forcing due to distortion in a boundary layer ingesting fan, J. Turbomach. 146 (7) (2024) 071008, https://doi.org/10.1115/1.4065517.
[10] Z. Altaf, M.I. Babar, S. Salamat, Multi-objective shape optimization of doubly offset serpentine diffuser using adjoint method, Int. J. Heat Fluid Flow 102 (2023) 109157, https://doi.org/10.1016/j.ijheatfluidflow.2023.109157.
[11] G.G. Lee, W.D.E. Allan, K. Goni Boulama, Flow and performance characteristics of an Allison 250 gas turbine s-shaped diffuser: effects of geometry variations, Int. J. Heat Fluid Flow 42 (2013) 151–163, https://doi.org/10.1016/j.ijheatfluidflow.2013.02.004.
[12] J.V. Taylor, F. Flanagan, A. Dunlop, S.D. Grimshaw, R.J. Miller, Super aggressive S-ducts for air breathing rocket engines, J. Turbomach. 143 (6) (2021) 061015, https://doi.org/10.1115/1.4050596.
[13] G. Tanguy, D.G. MacManus, E. Garnier, Numerical investigation of the unsteady distortion for an S-duct intake with mechanical vortex generators, Int. J. Heat Fluid Flow 95 (2022) 108975, https://doi.org/10.1016/j.ijheatfluidflow.2022.108975.
[14] M.M. Wojewodka, C. White, S. Shahpar, K. Kontis, A review of flow control techniques and optimisation in S-shaped ducts, Int. J. Heat Fluid Flow 74 (2018) 223–235, https://doi.org/10.1016/j.ijheatfluidflow.2018.06.016.
[15] P.K. Zachos, D.G. MacManus, D.G. Prieto, N. Chiereghin, flow distortion measurements in convoluted aeroengine intakes, AIAA J. 54 (9) (2016) 2819–2832, https://doi.org/10.2514/1.J054904.
[16] D.G. MacManus, N. Chiereghin, D.G. Prieto, P. Zachos, Complex aeroengine intake ducts and dynamic distortion, AIAA J. 55 (7) (2017) 2395–2409, https://doi.org/10.2514/1.J054905.
[17] D. Gil-Prieto, P.K. Zachos, D.G. MacManus, G. McLelland, Unsteady characteristics of S-duct intake flow distortion, Aerosp. Sci. Technol. 84 (1) (2019) 938–952, https://doi.org/10.1016/j.ast.2018.10.020.
[18] D. Gil-Prieto, D.G. MacManus, P.K. Zachos, G. Tanguy, K.R. Menzies, Convoluted intake distortion measurements using stereo particle image velocimetry, AIAA J. 55 (6) (2017) 1878–1892, https://doi.org/10.2514/1.J055467.
[19] M. Migliorini, P.K. Zachos, D.G. MacManus, P. Haladuda, S-duct flow distortion with non-uniform inlet conditions, Proc. Inst. Mech. Eng. G: J. Aerosp. Eng. (2022) 095441002211016, https://doi.org/10.1177/09544100221101669.
[20] M. Migliorini, P. Zachos, D. MacManus, An Assessment on the Unsteady Flow Distortion Generated by an S-Duct Intake, 2019, doi: 10.2514/6.2019-4201.
[21] K.U. Kempaiah, T. Piovesan, P.K. Zachos, D. Michaelis, R. Gebbink, B. Van Rooijen, D.G. Prieto, D. MacManus, A. Sciacchitano, C. Sheaf, High-resolution turbofan intake flow characterization by automated stereoscopic-PIV in an industrial wind tunnel environment, Meas. Sci. Technol. 35 (2) (2024) 025210, https://doi.org/10.1088/1361-6501/ad0ea0.
[22] T. Guimarães, K. Todd Lowe, W.F. O'Brien, Complex flow generation and development in a full-scale turbofan inlet, J. Eng. Gas Turbines Power 140 (8) (2018) 082606, https://doi.org/10.1115/1.4039179.
[23] T. Piovesan, P.K. Zachos, D.G. MacManus, K. Kempaiah, D. Michaelis, B. Van Rooijen, M. Vahdati, C. Sheaf, Coupled fan-intake dynamic distortion characterization at crosswind conditions, AIAA J. (2024) 1–5, https://doi.org/10.2514/1.J064595.
[24] B.K. Hodder, An Investigation of Engine Influence on Inlet Performance, NASA CR-166136, Seattle, WA, United States, 1981.
[25] D.L. Motycka, Reynolds number and fan/inlet coupling effects on subsonic transport inlet distortion, J. Propul. Power 1 (3) (1985) 229–234, https://doi.org/10.2514/3.22785.
[26] M.J. Larkin, P.S. Schweiger, Ultra High Bypass Nacelle Aerodynamics Inlet Flow-through High Angle of Attack Distortion Test, NASA CR-189149, United States, 1992.
[27] M. Carnevale, F. Wang, L. di Mare, Low frequency distortion in civil aero-engine intake, J. Eng. Gas Turbines Power 139 (4) (2017), https://doi.org/10.1115/1.4034600.
[28] T. Cao, N.R. Vadlamani, P.G. Tucker, A.R. Smith, M. Slaby, C.T.J. Sheaf, Fan–intake interaction under high incidence, J. Eng. Gas Turbines Power 139 (4) (2017), https://doi.org/10.1115/1.4034701.

[29] L. Boscagli, R. Christie, D. MacManus, T. Piovesan, Aerodynamics of a short intake in crosswind, Aerosp. Sci. Technol. 129 (2022) 107826, https://doi.org/10.1016/j.ast.2022.107826.
[30] E. Garnier, Flow control by pulsed jet in a curved S-duct: a spectral analysis, AIAA J. 53 (10) (2015) 2813–2827, https://doi.org/10.2514/1.J053422.
[31] M. Migliorini, P.K. Zachos, D.G. MacManus, U. Doll, M. Dues, S.J. Jonas, F. Dues, A. Siswanto, S.M. Melnikov, I. Rohle, Seeding-free inlet flow distortion measurements using filtered Rayleigh scattering: integration in a complex intake test facility, in: Presented at the AIAA SCITECH 2024 Forum, Orlando, FL, 2024, doi: 10.2514/6.2024-2831.
[32] M. Raffel, C.E. Willert, S.T. Wereley, J. Kompenhans, S. Willert, S.T. Wereley, J. Kompenhans, Particle image velocimetry: a practical guide, in: Particle Image Velocimetry, edited by Springer-Verlag, Springer, Berlin, 2007, pp. 203–241.
[33] B. Wieneke, PIV uncertainty quantification from correlation statistics, Meas. Sci. Technol. 26 (7) (2015), https://doi.org/10.1088/0957-0233/26/7/074002.
[34] M. Migliorini, Impact of Inlet Conditions on Unsteady Flow Distortion for Complex Aero-Engine Intakes, Ph. D. Dissertation. Cranfield University, UK, 2021.
[35] A Methodology for Assessing Inlet Swirl Distortion, Aerospace Information Report AIR 5686, Society of Automotive Engineers, Warrendale, PA, 2017, doi: 10.4271/AIR5686.
[36] Gas Turbine Engine Inlet Flow Distortion Guidelines, Aerospace Recommended Practice ARP1420C, Society of Automotive Engineers, Warrendale, PA, 2017.
[37] M. Migliorini, P.K. Zachos, D.G. MacManus, Novel method for evaluating intake unsteady flow distortion, J. Propul. Power (2021) 1–13, https://doi.org/10.2514/1.B38127.
[38] J.E. Giuliani, J.-P. Chen, Fan Response to boundary-layer ingesting inlet distortions, AIAA J. 54 (10) (2016) 3232–3243, https://doi.org/10.2514/1.J054762.
[39] M. Migliorini, P.K. Zachos, D. MacManus, Characterization of Unsteady Distortion Events for S-Duct Intakes under Non-Uniform Inlet Conditions, in: Presented at the AIAA SCITECH 2023 Forum, National Harbor, MD & Online, 2023, doi: 10.2514/6.2023-0502.
[40] A. Mehdi, Effect of Swirl Distortion on Gas Turbine Operability, PhD Thesis. Propulsion Engineering Centre, School of Aerospace, Transport and Manufacturing, Cranfield University, 2014.
[41] D.P. Welch, The Use of Fast Fourier Transform for the Estimation of Power Spectra: A Method Based on Time Averaging Over Short, Modified Periodograms, Vol. 15, 1967, pp. 70–73, doi: 10.1109/TAU.1967.1161901.